EMERGE

WP3

D3.1 Archetypes: Units and Connectors

Version: 1.0

Date: 27/09/2023

Funded by the European Union

European Innovation Council

Funded by the European Union under Grant Agreement 101070918. Views and opinions expressed are however those of the author(s) only and do not necessarily reflect those of the European Union or European Innovation Council and SMEs Executive Agency (EISMEA). Neither the European Union nor the granting authority can be held responsible for them.

Document control

Project title	Emergent awareness from minimal collectives
Project acronym	EMERGE
Call identifier	HORIZON-EIC-2021-PATHFINDERCHALLENGES-01-01
Grant agreement	101070918
Starting date	01/10/2022
Duration	48 months
Project URL	http://eic-emerge.eu
Work Package	WP3
Deliverable	D3.1
Contractual Delivery Date	30/09/2023
Actual Delivery Date	28/09/2023
Nature[1]	R
Dissemination level[2]	PU
Lead Beneficiary	TUD
Editor(s)	Maximilian Stölzle (TUD), Cosimo Della Santina (TUD)
Contributor(s)	Maximilian Stölzle (TUD), Jingyue Liu (TUD), Andrea Ceni (UNIPI), Andrea Cossu (UNIPI), Cosimo Della Santina (TUD)
Reviewer(s)	Davide Bacciu (UNIPI)
Document description	With this deliverable, we will present our preliminary investigations into Units and Connectors. Our ultimate goal is to define a set of building blocks that can be combined into more complex systems - called archetype networks - that are the fundamental computational engine of EMERGE. We build this framework using the language of nonlinear dynamical systems. As a result of T3.1, we discuss archetypical units, their definition, and a brief description of the dynamical systems we more closely looked at so far. Resulting from our investigations within T3.2, we then provide a similar

[1]R: Document, report (excluding the periodic and final reports); DEM: Demonstrator, pilot, prototype, plan designs; DEC: Websites, patents filing, press & media actions, videos, etc.; DATA: Data sets, microdata, etc.; DMP: Data management plan; ETHICS: Deliverables related to ethics issues.; SECURITY: Deliverables related to security issues; OTHER: Software, technical diagram, algorithms, models, etc.

[2]PU – Public, fully open, e.g. web (Deliverables flagged as public will be automatically published in CORDIS project's page); SEN – Sensitive, limited under the conditions of the Grant Agreement; Classified R-UE/EU-R – EU RESTRICTED under the Commission Decision No2015/444; Classified C-UE/EU-C – EU CONFIDENTIAL under the Commission Decision No2015/444; Classified S-UE/EU-S – EU SECRET under the Commission Decision No2015/444

Funded by the European Union

European Innovation Council

Funded by the European Union under Grant Agreement 101070918. Views and opinions expressed are however those of the author(s) only and do not necessarily reflect those of the European Union or European Innovation Council and SMEs Executive Agency (EISMEA). Neither the European Union nor the granting authority can be held responsible for them.

	analysis for the connectors. Subsequently, we derive the characteristics and stability properties of a few examples of archetypical networks. Importantly, this involves fundamental analysis within T3.2. Finally, we draw the connection to WP4 by stating how archetypes (and specifically archetypical networks) can be used as part of computing (T4.1) and adaptive systems (T4.3).

Funded by the European Union

European Innovation Council

Funded by the European Union under Grant Agreement 101070918. Views and opinions expressed are however those of the author(s) only and do not necessarily reflect those of the European Union or European Innovation Council and SMEs Executive Agency (EISMEA). Neither the European Union nor the granting authority can be held responsible for them.

Version control

Version[3]	Editor(s) Contributor(s) Reviewer(s)	Date	Description
0.1	Cosimo Della Santina	06/07/2023	TOC draft
0.2	Maximilian Stölzle, Jingyue Liu, Cosimo Della Santina	31/07/2023	Preliminary draft of archetypes and connectors
0.3	Maximilian Stölzle, Jingyue Liu, Andrea Cossu, Andrea Ceni	10/08/2023	Examples of archetype networks
0.4	Maximilian Stölzle, Jingyue Liu, Andrea Cossu, Andrea Ceni, Cosimo Della Santina	31/08/2023	First complete draft of the report
0.5	Maximilian Stölzle	21/09/2023	Report released for internal review
1.0	Davide Bacciu, Cosimo Della Santina	27/09/2023	Report updated with internal review comments. Ready for submission.

[3] 0.1 – TOC proposed by editor; 0.2 – TOC approved by reviewer; 0.4 – Intermediate document proposed by editor; 0.5 – Intermediate document approved by reviewer; 0.8 – Document finished by editor; 0.85 – Document reviewed by reviewer; 0.9 – Document revised by editor; 0.98 – Document approved by reviewer; 1.0 – Document released by Project Coordinator.

Funded by the European Union

European Innovation Council

Funded by the European Union under Grant Agreement 101070918. Views and opinions expressed are however those of the author(s) only and do not necessarily reflect those of the European Union or European Innovation Council and SMEs Executive Agency (EISMEA). Neither the European Union nor the granting authority can be held responsible for them.

Abstract

With this deliverable, we will present our preliminary investigations into Units and Connectors. Our ultimate goal is to define a set of building blocks that can be combined into more complex systems - called archetype networks - that are the fundamental computational engine of EMERGE. We build this framework using the language of nonlinear dynamical systems.

The document sections are organized as follows. We start by discussing the units, their definition, and a brief description of the systems we more closely looked at so far. We then provide a similar analysis for the connectors. Subsequently, we derive the characteristics and stability properties of a few examples of archetypical networks. Finally, we draw the connection to WP4 by stating how archetypes can be used as part of computing and adaptive systems.

Funded by the European Union

European Innovation Council

Funded by the European Union under Grant Agreement 101070918. Views and opinions expressed are however those of the author(s) only and do not necessarily reflect those of the European Union or European Innovation Council and SMEs Executive Agency (EISMEA). Neither the European Union nor the granting authority can be held responsible for them.

Disclaimer

Acknowledgement

This document is a deliverable of EMERGE project. This project has received funding from the European Union's Horizon Europe research and innovation programme under grant agreement Nº 101070918.

Table of Contents

List of abbreviations

WP	Work package
ODE	Ordinary Differential Equation
PDM	Position-dependent Mass

Funded by the European Union

European Innovation Council

Funded by the European Union under Grant Agreement 101070918. Views and opinions expressed are however those of the author(s) only and do not necessarily reflect those of the European Union or European Innovation Council and SMEs Executive Agency (EISMEA). Neither the European Union nor the granting authority can be held responsible for them.

1. Units

1.1 Definition

An archetypical unit is an ODE of form $\dot{y}_i = f(y_i, u_i)$ where $y_i \in R^n$ is the state of the unit and $u_i \in R$ a scalar input. We emphasize that n is of relatively small dimension. In all the units we discuss below, n = 2, as y_i can be interpreted as the position and velocity of a (pseudo-) mechanical system.

1.2 Harmonic oscillator

The three fundamental components of a mechanical system are potential energy and kinetic energy storage units (e.g., springs and masses respectively), and sources of energy dissipation (e.g., dampers). The simplest interconnection of one element of each class generates a mechanical oscillator, which we show in Fig. 1.

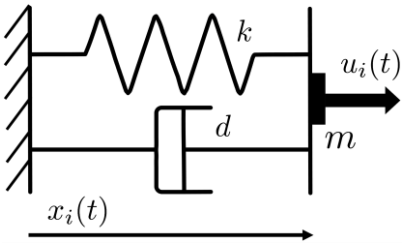

Figure 1: Schematic representation of a harmonic oscillator.

If the characteristics of the spring and the damper is linear and the mass is constant, the oscillator is called harmonic and it is described by the following ODE, where we also include a time-varying forcing $u_i(t)$:

$$m\,\ddot{x}_i + k\,x_i + d\,\dot{x}_i = u_i$$

Here, $x_i(t)$, $x_i\dot{(t)}$, $\ddot{x}_i(t) \in R$ are the configuration, velocity, and acceleration of the oscillator respectively. The point mass attached to the end of the oscillator is denoted with $m \in R^+$, the spring stiffness with $k \in R^+$, and the damping coefficient with $d \in R^+$. The state of this 2nd order ODE is defined as $y_i = [x_i\ \dot{x}_i]^T \in R^2$. The equilibrium of the system is given by $\bar{y}_i = [0\ 0]^T$.

First, we consider the unforced system $u_i(t) = 0$ with a stable equilibrium in $\bar{x}_i = 0$, for which the choice of initial conditions $x(0), \dot{x}(0)$ give rise to different transient solutions. The linear elastic forces $\tau_{el} = -k\,x_i$ relate to the intrinsic frequency of the underlying harmonic oscillator. A key feature required for a dynamical system to be exploited for computational purposes is the *fading memory*. In rough terms, we aim for a stable dynamical system that can forget the initial condition after a transient. Fading memory can be established with damping coefficient $d > 0$, thus introducing a source of energy dissipation and inducing the system to converge towards the resting state of $x_i = 0$ which we visualize with the orange line in Fig. 3.

Funded by the European Union

European Innovation Council

Funded by the European Union under Grant Agreement 101070918. Views and opinions expressed are however those of the author(s) only and do not necessarily reflect those of the European Union or European Innovation Council and SMEs Executive Agency (EISMEA). Neither the European Union nor the granting authority can be held responsible for them.

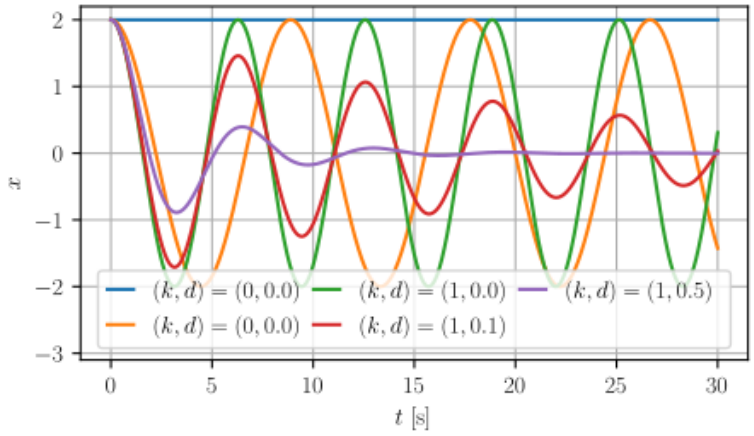

Figure 2: Time evolution of a harmonic oscillator for different stiffness and damping coefficients. The point mass is always chosen to be $m = 1$.

In Figure 1, we present the time evolution of a harmonic oscillator for different parameters. The stiffness determines the frequency of the oscillation (see blue, orange, and green lines). If a damping coefficient larger than zero is chosen, then the configuration of the oscillator converges towards the equilibrium $\bar{x}_i = 0$.

1.3 Multistable oscillator

The harmonic oscillator can exhibit multistable characteristics by adding a nonlinear potential:

$$m\,\ddot{x}_i + k\,x_i + d\,\dot{x}_i + \tanh(w\,x_i + b) = u_i$$

where $w \in R^-$, and $b \in R$. This characteristic might be desirable for hybrid systems where the initial condition should have an impact on the output of the network.

We analyse the equilibria of the unforced system ($u_i = 0$). For $b = 0$, the system always has a single equilibrium at $\bar{x} = 0$. If $b \neq 0$ and $w = 0$, the system has a single equilibrium at $\bar{x} = \frac{tanh(b)}{k}$. On the other hand, if $b \neq 0$ and $W < 0$, the system becomes multistable for certain choices of b. Namely, the system can have between one and three equilibria. If the oscillator has only one equilibrium (as seen in Fig. 3), it will be asymptotically stable. For two equilibria (shown in Fig. 4), one will be unstable and the other one will be asymptotically stable. If the system has three equilibria, two of them will be asymptotically and the other one unstable as it is shown in Fig. 5. It is important to note that all equilibria will be within the interval $[-1,1]$.

We remark that this unit is equivalent to the scalar case of a network of harmonic oscillators coupled to each other by the neuron-like connector.

Funded by the European Union

European Innovation Council

Funded by the European Union under Grant Agreement 101070918. Views and opinions expressed are however those of the author(s) only and do not necessarily reflect those of the European Union or European Innovation Council and SMEs Executive Agency (EISMEA). Neither the European Union nor the granting authority can be held responsible for them.

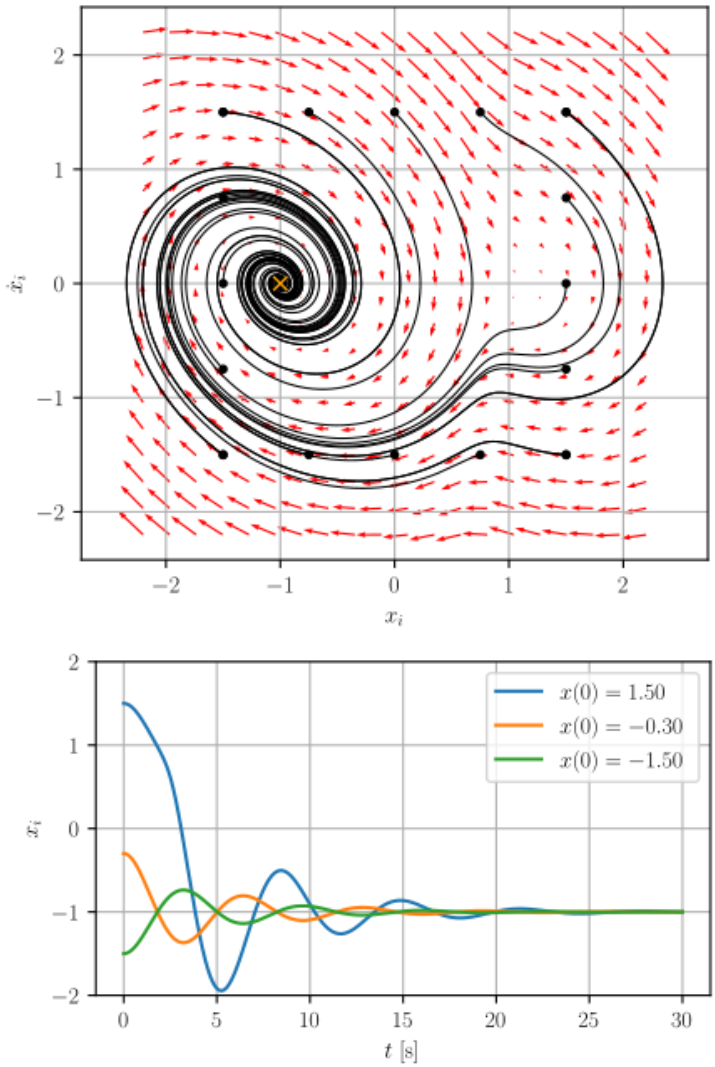

Figure 3: Phase portrait and time evolution of a one-dimensional harmonic oscillator with neural coupling and a single, asymptotically stable equilibrium at $\bar{x} = -1$. The oscillator is configured with $k = 1$, $d = 0.4$, $w = -5$, $b = 4$, and $u = 0$. The orange cross in the phase portrait denotes the equilibrium state. Furthermore, we display on the phase portrait sample trajectories (solid black lines) with their initial condition marked with a black dot.

Funded by the European Union

European Innovation Council

Funded by the European Union under Grant Agreement 101070918. Views and opinions expressed are however those of the author(s) only and do not necessarily reflect those of the European Union or European Innovation Council and SMEs Executive Agency (EISMEA). Neither the European Union nor the granting authority can be held responsible for them.

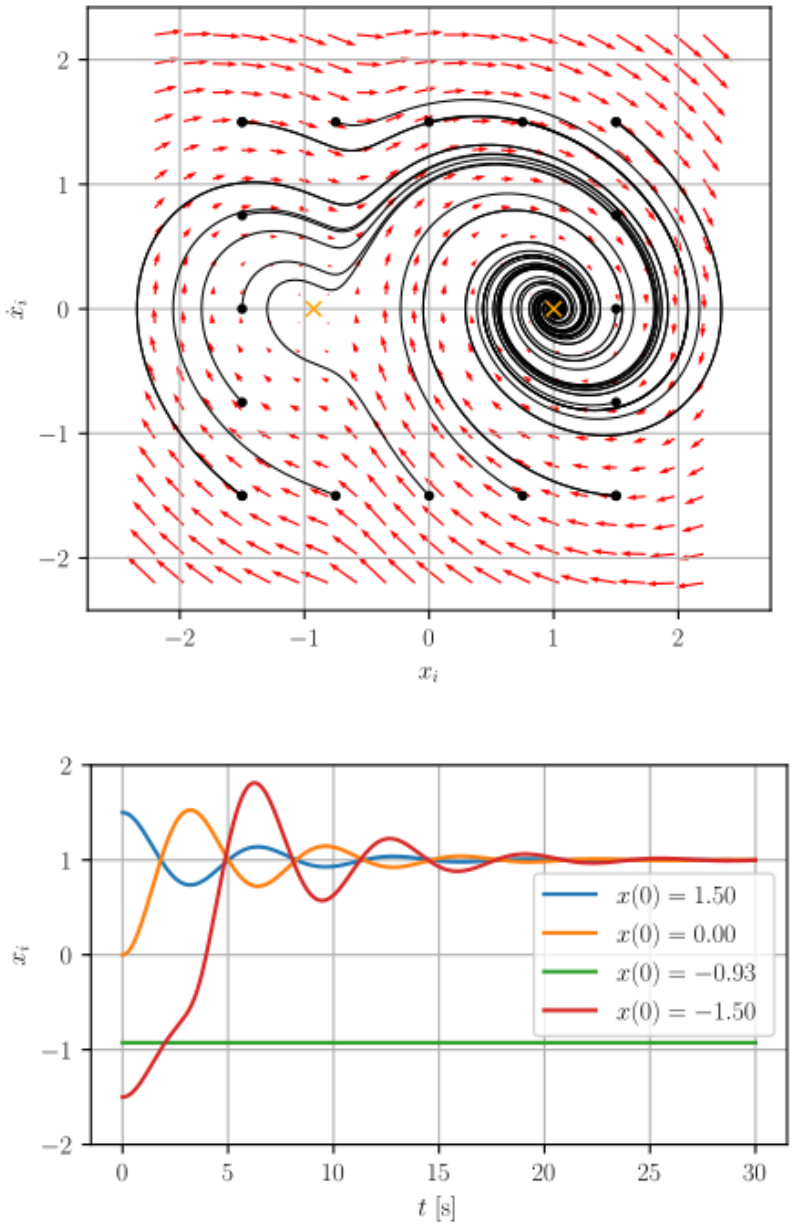

Figure 4: Phase portrait and time evolution of a one-dimensional harmonic oscillator with neural coupling. The oscillator has two equilibria: one asymptotically stable equilibrium at $\bar{x}_1 = 1$ and one unstable equilibrium at $\bar{x}_2 = -0.93$. The oscillator is configured with $k = 1$, $d = 0.4$, $w = -5$, $b = -3$, and $u = 0$. The orange crosses in the phase portrait denote the equilibrium states. Furthermore, we display on the phase portrait sample trajectories (solid black lines) with their initial condition marked with a black dot.

Funded by the European Union

European Innovation Council

Funded by the European Union under Grant Agreement 101070918. Views and opinions expressed are however those of the author(s) only and do not necessarily reflect those of the European Union or European Innovation Council and SMEs Executive Agency (EISMEA). Neither the European Union nor the granting authority can be held responsible for them.

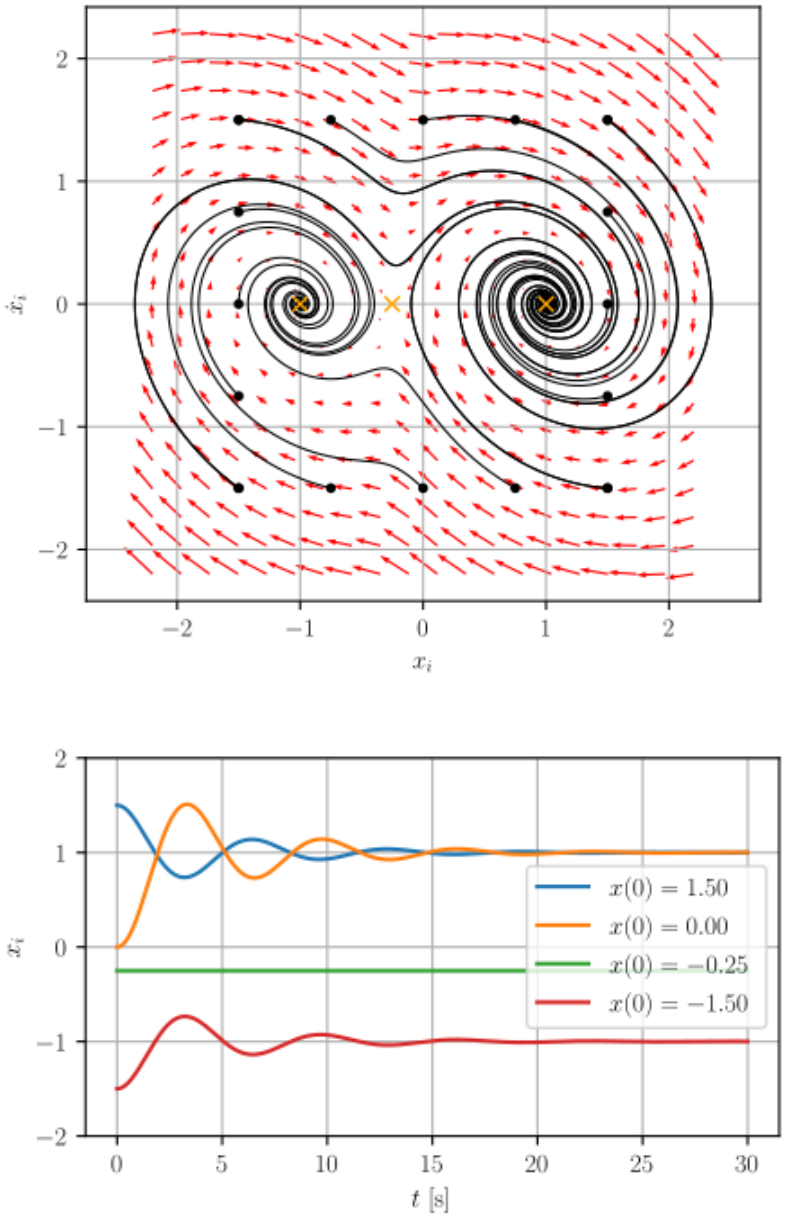

Figure 5: Phase portrait and time evolution of a one-dimensional, multistable harmonic oscillator with neural coupling for the case of $k = 1$, $d = 0.4$, $w = -5$, $b = -1$, and $u = 0$. The oscillator exhibits three equilibria: two asymptotically stable equilibria at $\bar{x}_1 = 1$ and $\bar{x}_2 = -1$, and finally an unstable equilibrium at $\bar{x}_3 = -0.25$. The input is deactivated with $u = 0$. The orange crosses in the phase portrait denote the equilibrium states. Furthermore, we display on the phase portrait sample trajectories (solid black lines) with their initial condition marked with a black dot.

1.4 Oscillator with position-dependent mass

Oscillators with position-dependent mass (PDM) have great importance in many branches of physics and impart more complexity and richness to the dynamics. The equation of motion governing such oscillators is

$$m(x_i)\,\ddot{x}_i + c(x_i, \dot{x}_i)\dot{x}_i + d\dot{x}_i + kx_i = u_i,$$

Funded by the European Union

European Innovation Council

Funded by the European Union under Grant Agreement 101070918. Views and opinions expressed are however those of the author(s) only and do not necessarily reflect those of the European Union or European Innovation Council and SMEs Executive Agency (EISMEA). Neither the European Union nor the granting authority can be held responsible for them.

where the function $m(x_i)$ characterizes the position-dependent mass. This equation is the Euler-Lagrange equation for the Lagrangian

$$L(x_i, \dot{x}_i) = \frac{1}{2} m(x_i)\dot{x_i}^2 - \frac{1}{2}kx_i^2$$

The Coriolis component, $c(x_i, \dot{x}_i)$, arise from the time derivative of the mass, $m(x_i)$, as

$$c(x_i, \dot{x}_i) = \frac{1}{2}\dot{m}(x_i)$$

for the one-dimension case.

An often-used generalization of the one-dimension PDM oscillator was proposed by Mathew and Lakshmanan (P. M. and M. 1974) as

$$\left(1 + \lambda x_i^2\right)\ddot{x}_i - \lambda x_i \dot{x}_i^2 + \alpha^2 x_i = 0$$

Where $\lambda > 0$ and α are the parameters of the system. The position-dependent mass $m(x)$ depends on

$$m(x_i) = \frac{1}{1 + \lambda x_i^2}$$

Under specific conditions, this oscillator exhibits remarkable simplicity at fixed frequencies and amplitudes, resembling the behaviour of a simple harmonic oscillator.

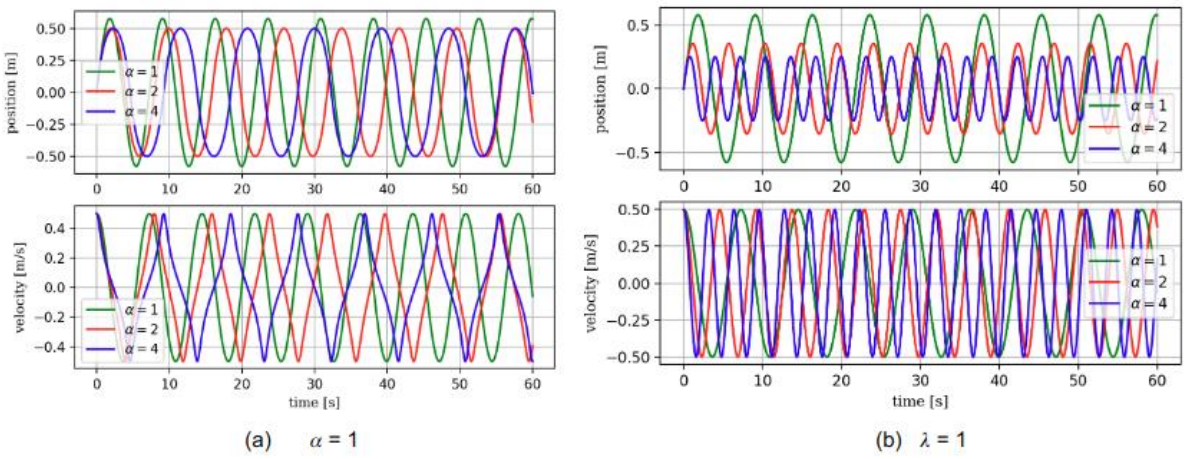

Figure 6: Time evolution of the example position-dependent mass oscillator from the initial state (0.0, 0.5): (a) shows motion with different λ values (b) shows motion with different α values.

Funded by the European Union

European Innovation Council

Funded by the European Union under Grant Agreement 101070918. Views and opinions expressed are however those of the author(s) only and do not necessarily reflect those of the European Union or European Innovation Council and SMEs Executive Agency (EISMEA). Neither the European Union nor the granting authority can be held responsible for them.

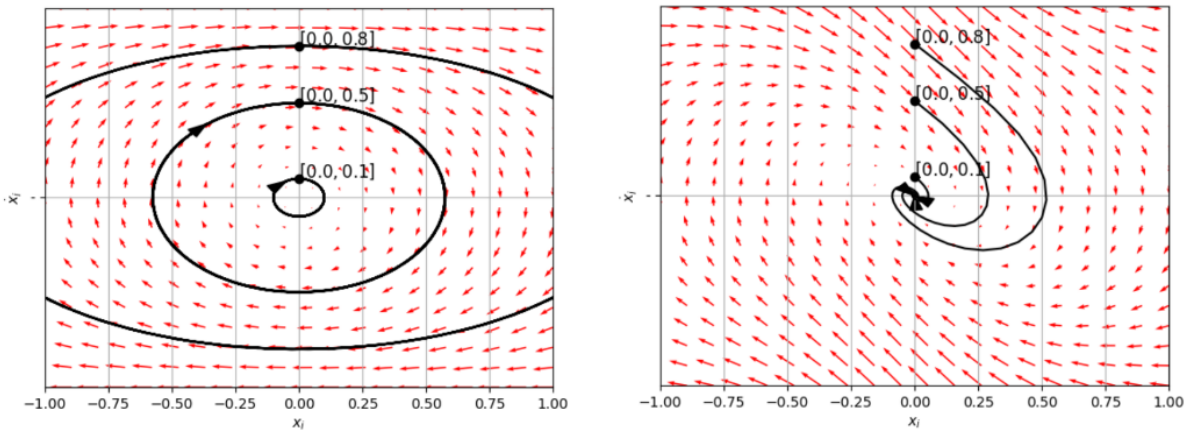

(a) PDM-oscillator without dissipation

(b) PDM-oscillator with dissipation

Figure 7: Phase portrait of the example position-dependent mass oscillator from different initial states: (a) shows the case without the dissipation (b)shows the scenario with dissipation.

Funded by the European Union

European Innovation Council

Funded by the European Union under Grant Agreement 101070918. Views and opinions expressed are however those of the author(s) only and do not necessarily reflect those of the European Union or European Innovation Council and SMEs Executive Agency (EISMEA). Neither the European Union nor the granting authority can be held responsible for them.

2 Connectors

2.1 Definition

We define a connector c as a map from the network states $y_v \in R^{n_v}$ and the global network inputs $v_S \in R^{n_s}$ to the scalar input $u_i \in R$ for the *i*th unit:

$$c : (y_{\mathcal{V}}, v_{\mathcal{S}}) \mapsto u_i$$

Here, V is a set of state indices and S a set of network input indices.

Therefore, connectors take the state of a subset of all units and a subset of all global inputs and map them in the input of one unit.

2.2 Neuron-like connector

This connector takes inspiration from neural networks and is defined as

$$u_i = \sigma\left(\sum_{j \in \mathcal{V}} W_{ij}\, y_j + \sum_{k \in \mathcal{S}} E_{ik}\, v_k + b_i\right)$$

where $\sigma: R \to R$ is an activation function, $W \in R^{n\,x\,n_v}$ is the state-to-state coupling matrix for all units in the set V and $E \in R^{n\,x\,n_s}$ maps the inputs of the set S to units in the set V. Furthermore, $b_i \in R$ is a bias constant.

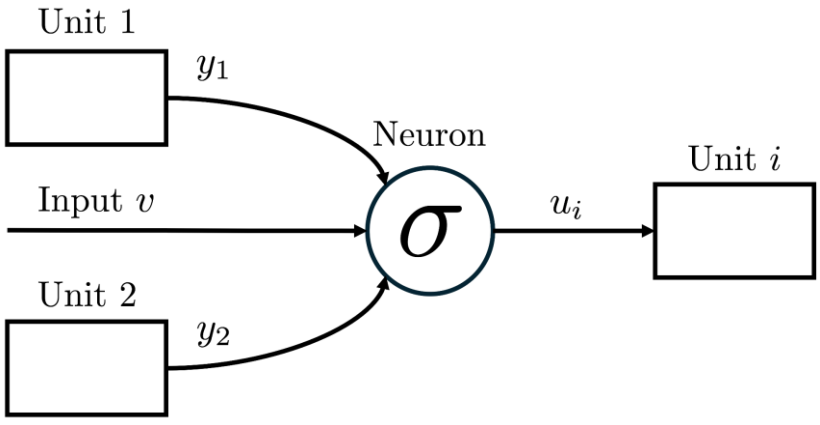

Figure 7: Circuital scheme of a neuron-like connector.

2.3 Potential coupling

Potential energy often arises from interactions with external systems or forces. It signifies the energy associated with the arrangement of a system's components within the influence of external factors and relies on its relationship with its environment or interactions with other

Funded by the European Union

European Innovation Council

Funded by the European Union under Grant Agreement 101070918. Views and opinions expressed are however those of the author(s) only and do not necessarily reflect those of the European Union or European Innovation Council and SMEs Executive Agency (EISMEA). Neither the European Union nor the granting authority can be held responsible for them.

systems. Building upon it, we introduce the concept of potential coupling forces to connect units. It defined as

$$u_i = \frac{\partial U}{\partial x_i} = \sum_{j \in \nu} u_{ij}$$

where U denotes the complete potential energy of the system, and u_i signifies the potential forces affecting unit i. This potential energy often includes stiffness potential energy between units and the inherent gravitational potential energy of each unit. Mathematically, U can be represented as a function of the configuration of units as

$$U = f(x_1, x_2, \ldots, x_{n_v}) .$$

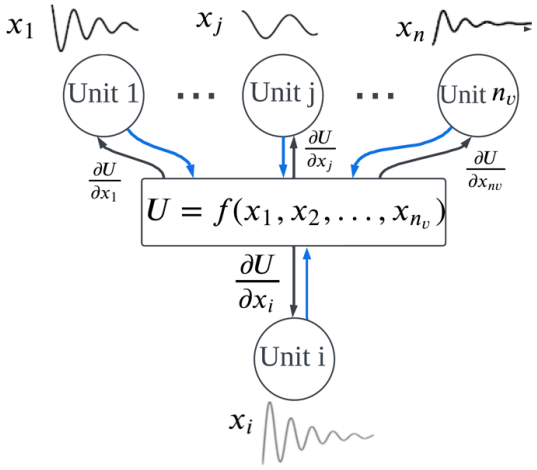

Figure 8: Scheme of the potential coupling connector.

2.4 Hyperbolic potential with perturbation

This connector is a specific subcase of the potential coupling. It takes loose inspiration from the structure of computational neurons while specializing in hyperbolic tangent activation functions. The connector mapping is given by

$$u_i = -\tanh\left(\sum_{j \in \mathcal{V}} W_{ij}\, y_j + b_i\right) + \tanh\left(\sum_{k \in \mathcal{S}} E_{ik}\, v_k\right)$$

where we define $W \succ 0$ as a positive-definite state-to-state coupling matrix, $b \in R^n$ as the bias vector, and $E \in R^{n\,x\,n_s}$ as the input-to-state mapping. The similarity to the neuron-like connector is obvious. The two differences are that a) the input is separate from the potential coupling, and b) that we assume W to be positive-definite and with that also to be symmetric. That results in a bi-directional potential coupling between the units.

Funded by the European Union

European Innovation Council

Funded by the European Union under Grant Agreement 101070918. Views and opinions expressed are however those of the author(s) only and do not necessarily reflect those of the European Union or European Innovation Council and SMEs Executive Agency (EISMEA). Neither the European Union nor the granting authority can be held responsible for them.

3 Examples of archetype networks

3.1 A network of harmonic oscillators with hyperbolic potential coupling

Summary: This network combines the harmonic oscillator unit with a hyperbolic potential connector. While we impose certain constraints on the parameters such as positive stiffness and damping coefficients and a positive definite state-to-state coupling matrix W, the design space is still quite large and allows for a large variety of different dynamical behaviours. With the use of Lyapunov arguments, we can provide strong stability guarantees for the oscillator network. Furthermore, this network is physically implementable by connecting oscillators with nonlinear stiffness with linear spring-damper elements to each other.

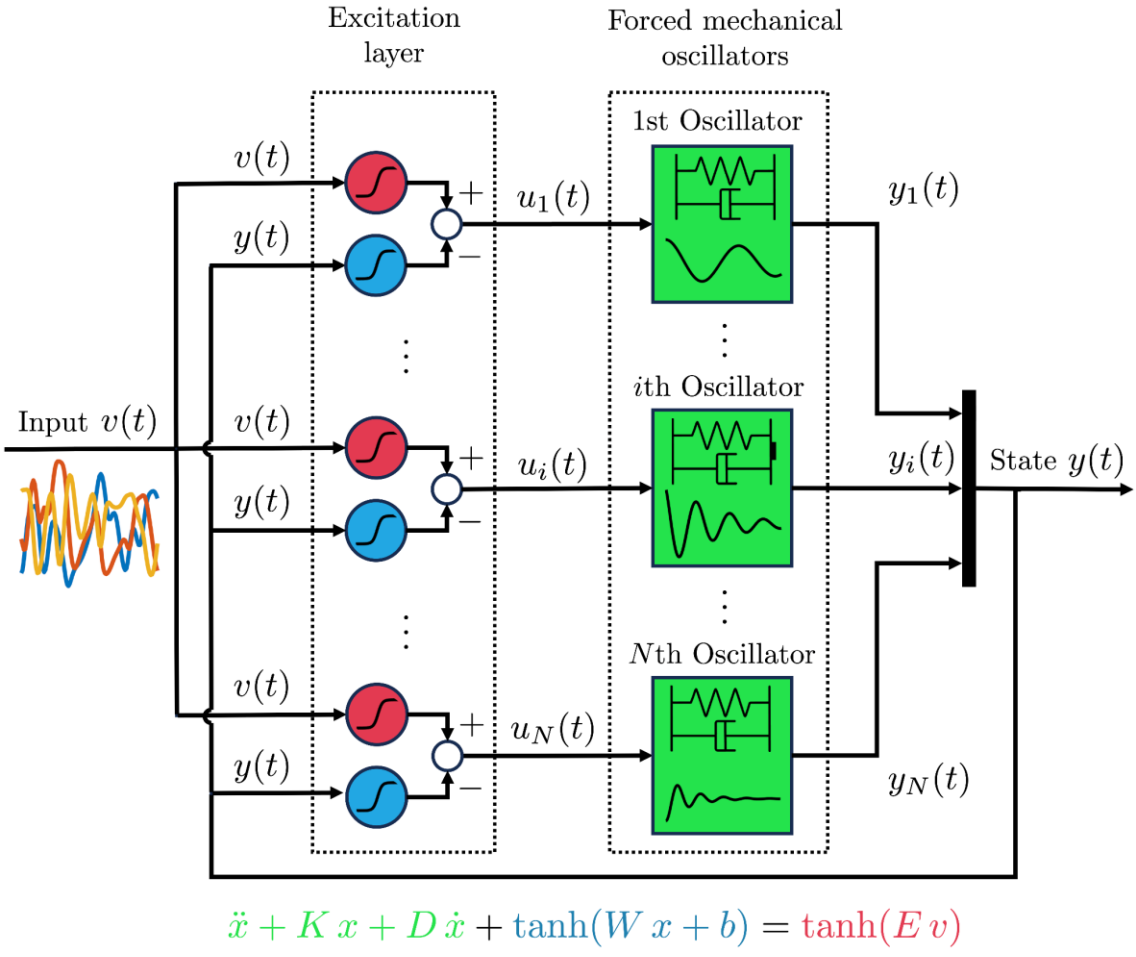

Figure 9: Block diagram of a network of harmonic oscillators with hyperbolic potential coupling.

Definition: The dynamics of a network of N oscillators with hyperbolic potential coupling is given by

$$\ddot{x} + K\,x + D\,\dot{x} + \tanh(W\,x + b) = \tanh(E\,v)$$

Funded by the European Union

European Innovation Council

Funded by the European Union under Grant Agreement 101070918. Views and opinions expressed are however those of the author(s) only and do not necessarily reflect those of the European Union or European Innovation Council and SMEs Executive Agency (EISMEA). Neither the European Union nor the granting authority can be held responsible for them.

where $x, \dot{x} \in R^N$ are the position and velocity of the oscillators respectively. With $K = diag(k_1, \ldots, k_i, \ldots, k_N)$ where $k_i > 0$, we describe the linear elasticity of the harmonic oscillators. $D = diag(d_1, \ldots, d_i, \ldots, d_N)$ are the strictly positive damping coefficients of the harmonic oscillators. We define $W \in R^{NxN} \succ 0$ as the positive-definite state-to-state coupling and $b \in R^N$ as the bias of the hyperbolic potential. The system is actuated by the bounded function $tanh(E\ v)$ where $E \in R^{NxN}$.

Characterization: The unactuated system with $v(t) = 0$ always has one globally asymptotically stable equilibrium $\bar{y} = [\bar{x}, 0]^T$ at the root of the equation $K\bar{x} + tanh(W\bar{x} + b) = 0$. We visualize the time evolution of an unactuated network of three units in Fig. 8.

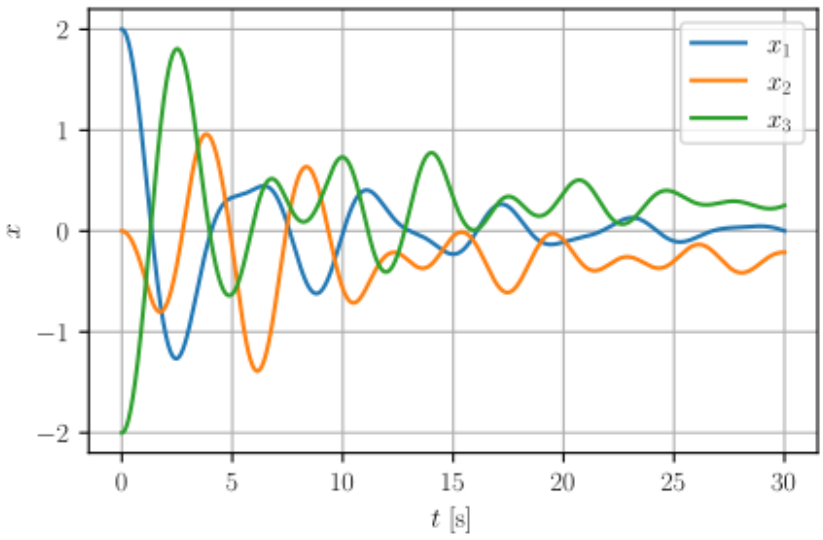

Figure 10: Evolution of a network of three harmonic oscillators connected by hyperbolic potential coupling and $v(t) = [0,0,0]$. *We choose* $K = diag(1,1,1), D = diag(0.2, 0.2, 0.2)$, $W = [2.0, 1.0, 1.0;\ 1.0, 2.0, -0.5, 1.0, -0.5, 2.0]$, *and* $b = [0, 1, -1]$.

We can provide a proof of Input-to-State (ISS) stability (Khalil 2002, 174) using strict Lyapunov arguments (Wu et al. 2022). First, we conduct a change of variables: $y_w = W\ (y - \bar{y})$. We define $\bar{x}_w = W\ \bar{x}$, $B_w = W^{-1} \succ 0$, $K_w = K\ W^{-1}$, and $D_w = D\ W^{-1}$ and assume $K_w \succ 0$, $D_w \succ 0$. Now, the system becomes

$$\frac{\mathrm{d}x}{\mathrm{d}t} = \dot{x}$$

$$\frac{\mathrm{d}\dot{x}}{\mathrm{d}t} = B_{\mathrm{w}}^{-1}\left(-\tanh(\bar{x}_{\mathrm{w}} + x_{\mathrm{w}} + b) - K_{\mathrm{w}}\ (\bar{x}_{\mathrm{w}} + x_{\mathrm{w}}) - D_{\mathrm{w}}\ \dot{x}_{\mathrm{w}} + \tanh(E\ v)\right)$$

Consider now the strict Lyapunov candidate with skewed level sets

$$V_\mu(y_{\mathrm{w}}) = \frac{1}{2}\, y_{\mathrm{w}}^{\mathrm{T}}\, P_{\mathrm{V}}\, y_{\mathrm{w}} + \sum_{i=1}^{N} \int_0^{x_{\mathrm{w}}} \tanh(\bar{x}_{\mathrm{w},i} + \sigma + b_i)\, \mathrm{d}\sigma - \sum_{i=1}^{N} \int_0^{x_{\mathrm{w}}} \tanh(\bar{x}_{\mathrm{w},i} + b_i)\, \mathrm{d}\sigma$$

where

Funded by the European Union

European Innovation Council

Funded by the European Union under Grant Agreement 101070918. Views and opinions expressed are however those of the author(s) only and do not necessarily reflect those of the European Union or European Innovation Council and SMEs Executive Agency (EISMEA). Neither the European Union nor the granting authority can be held responsible for them.

$$P_{\mathrm{V}} = \begin{bmatrix} K_{\mathrm{w}} & \mu\, B_{\mathrm{w}} \\ \mu\, B_{\mathrm{w}}^{\mathrm{T}} & B_{\mathrm{w}} \end{bmatrix}$$

The strict Lyapunov candidate is valid for any μ satisfying

$$0 < \mu < \frac{\sqrt{\lambda_{\mathrm{m}}(B_{\mathrm{w}})\, \lambda_{\mathrm{m}}(K_{\mathrm{w}} + S_{\mathrm{sech}}^2)}}{\|B_{\mathrm{w}}\|} := \mu_{\mathrm{V}}$$

where $\lambda_m(A)$, and $\lambda_M(A)$ are the minimum and maximum Eigenvalues and $||A||$ the induced norm of the matrix A. Here, we also defined $S_{sech}(y_w) = diag(sech(\underline{x}_w + x_w + b)) \succeq 0$. The Lyapunov candidate is bounded by

$$\frac{1}{2}\, \lambda_{\mathrm{m}}(P_{\mathrm{V}})\, \|y_{\mathrm{w}}\|_2^2 \leq V_\mu(y_{\mathrm{w}}) \leq \frac{1}{2}\, \lambda_{\mathrm{M}}(P_{\mathrm{V}})\, \|y_{\mathrm{w}}\|_2^2 + 2\sqrt{N}\|y_{\mathrm{w}}\|_2$$

The time derivative of the Lyapunov candidate becomes

$$\dot{V}_\mu(y_{\mathrm{w}}) \leq -\lambda_{\mathrm{m}}(P_{\dot{V}})\, \|y_{\mathrm{w}}\|_2^2 + \|y_{\mathrm{w}}^{\mathrm{T}}\, F_{y_{\mathrm{w}}}^{v}\|_1$$

where $F_{y_w}^v = [\mu\, tanh\,(Ev)^T,\, tanh\,(Ev)^T]^T$ and

$$P_{\dot{V}} = \begin{bmatrix} \mu\, K_{\mathrm{w}} & \frac{1}{2}\, \mu\, D_{\mathrm{w}} \\ \frac{1}{2}\, \mu\, D_{\mathrm{w}}^{\mathrm{T}} & D_{\mathrm{w}} - \mu\, B_{\mathrm{w}} \end{bmatrix} \succ 0$$

if

$$0 < \mu < \frac{\lambda_{\mathrm{m}}(D_{\mathrm{w}})}{\lambda_{\mathrm{m}}(D_{\mathrm{w}}) + \frac{\|D_{\mathrm{w}}\|^2}{4\, \lambda_{\mathrm{m}}(K_{\mathrm{w}})}} := \mu_{\dot{V}}$$

We conclude that there always exists a μ satisfying $0 < \mu < min\{\mu_V, \mu_{\dot{V}}\}$. We now aim to dominate the input with the quadratic term to demonstrate ISS stability. It follows with $0 < \theta < 1$ and

$$\forall \|y_{\mathrm{w}}\|_2 \geq \frac{\sqrt{1+\mu^2}}{\theta\, \lambda_{\mathrm{m}}(P_{\dot{V}})}\, \|\tanh(Eu(t))\|_2 = \rho$$

that

$$\dot{V}_\mu(y_{\mathrm{w}}) \leq -(1-\theta)\lambda_{\mathrm{m}}(P_{\dot{V}})\, \|y_{\mathrm{w}}\|_2^2$$

Funded by the European Union

European Innovation Council

Funded by the European Union under Grant Agreement 101070918. Views and opinions expressed are however those of the author(s) only and do not necessarily reflect those of the European Union or European Innovation Council and SMEs Executive Agency (EISMEA). Neither the European Union nor the granting authority can be held responsible for them.

Then, the system is ISS stable such that

$$\|y_{\mathrm{w}}\|_2 \leq \beta(\|y_{\mathrm{w}}(t_0)\|_2, t - t_0) + \gamma(\sup_{t \geq t_0} \|\tanh(E\, v(t)\|_2)$$

where $\gamma(r)$ is given by

$$\gamma(r) = \sqrt{\frac{(1+\mu^2)\,\lambda_{\mathrm{M}}(P_{\mathrm{V}})\,r^2 + 4\,\theta\sqrt{N}\sqrt{1+\mu^2}\,\lambda_{\mathrm{m}}(P_{\dot{\mathrm{V}}})\,r}{\theta^2\,\lambda_{\mathrm{m}}(P_{\mathrm{V}})\,\lambda_{\mathrm{m}}(P_{\dot{\mathrm{V}}})^2}}$$

3.2 A network of harmonic oscillators with neural coupling

Summary: This archetypical network combines harmonic oscillators with a neuron-like connector. It exhibits a high degree of expressiveness in terms of dynamical behaviours by the means of choosing the parameters of the oscillator and the neuron-like connector. A unique feature of this network is that it represents both a multi-stable system and a single-stable system depending on the choice of the state-to-state coupling W and the bias term b. Additionally, we notice mixed, nonlinear terms between the actuation and the neural coupling. One disadvantage of the formulation is that it is challenging to prove input-to-state stability of the system.

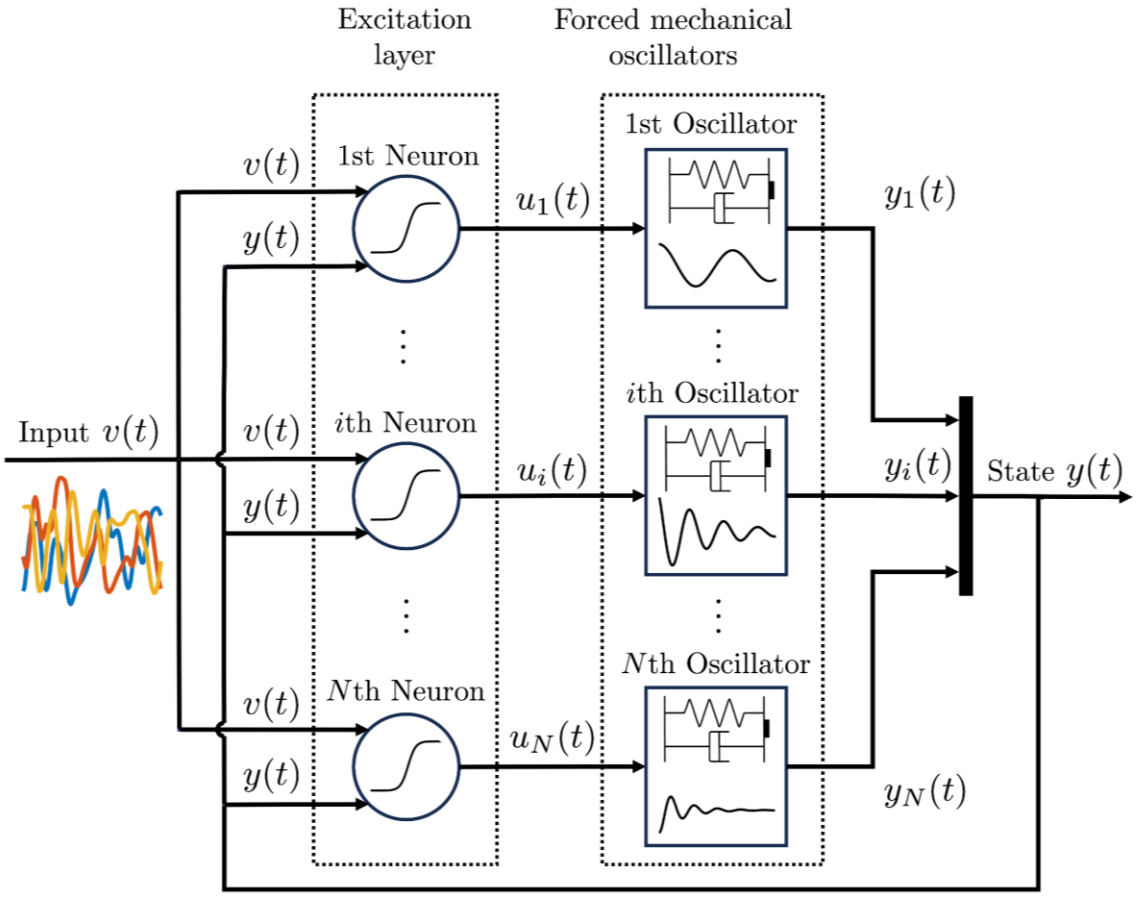

Funded by the European Union

European Innovation Council

Funded by the European Union under Grant Agreement 101070918. Views and opinions expressed are however those of the author(s) only and do not necessarily reflect those of the European Union or European Innovation Council and SMEs Executive Agency (EISMEA). Neither the European Union nor the granting authority can be held responsible for them.

Figure 11: Block diagram of a network of harmonic oscillators with neural coupling. A neuron with tanh activation function computes as a function of the current position and input $v(t)$the external forcing $u_i(t)$ to the harmonic oscillator with stiffness k_i and damping coefficient d_i.

Definition: The nonlinear state space dynamics of a network of N harmonic oscillators with neural coupling are given by

$$\ddot{x} + K\,x + D\,\dot{x} = \tanh(W\,x + E\,v + b)$$

where $x,\ \dot{x} \in R^N$ are the position and velocity of the oscillators respectively. With $K = diag(k_1,\dots,k_i,\dots,k_N)$, where $k_i > 0$, we describe the linear elasticity of the harmonic oscillators. $D = diag(d_1,\dots,d_i,\dots,d_N)$ are the strictly positive damping coefficients of the harmonic oscillators. We define $W \in R^{NxN}$ as the weight and $b \in R^N$ as the bias of the computational neuron. This term is mixed with the linearly mapped input $E\ v(t)$ where $E \in R^{NxN}$.

Characterization: First, we analyse the equilibria of the unactuated archetypical unit ($v(t) = 0$). For $b = 0$, the always has a single equilibrium at $\bar{x} = 0$. If $b \neq 0$ and $W = 0$, the system has a single equilibrium at $\bar{x} = K^{-1}\,b$. Furthermore, if $b \neq 0$ and $W \succ 0$, the system has again one equilibrium. Finally, if $b \neq 0$ and $W \preccurlyeq 0$, the system becomes multistable for certain choices of b.

To perform a stability analysis of the archetypical network at hand, we applied a widely known technique in the context of Reservoir Computing (RC) systems (Ceni, et al. 2023). Specifically, we impose the linearised system to be a contraction mapping. Namely, we impose the Euclidean norm of the Jacobian to be less than 1. This condition is sufficient to imply the existence and uniqueness of a uniformly asymptotically stable input-driven solution. We derived the following result:

$$||J_k|| \leq \max(\eta + \tau^2\sigma,\ \xi) + \tau\,\max(\xi,\ \gamma_{\max} + \sigma).$$

In such upper bound, τ is the discretisation time step, while $\xi = \max_j |1 - \tau\,d_j|$, $\eta = \max_j |1 - \tau^2\,k_j|$, $\gamma_{max} = \max_j k_j$, and $\sigma = ||W||$. However, imposing such a strong stability condition of contractivity constrains the archetypical unit on a too narrow region of hyperparameters, effectively compromising the expressive power of the model. Therefore, although not sufficient for ensuring stability, we looked for weaker necessary conditions for stability based on the eigenvalues distribution of the linearised system. We demonstrated the following result.

Theorem. For all μ eigenvalues of the linearised system, there exists a point $\lambda \in \{1 - \tau^2\,k_j\,,\ 1 - \tau\,d_j\}_{j=1}^{N}$ such that

$$|\mu - \lambda| \leq C,$$

where $C = \tau^2\sigma + \tau\,\max(\xi,\ \gamma_{max} + \sigma)$.

Funded by the European Union

European Innovation Council

Funded by the European Union under Grant Agreement 101070918. Views and opinions expressed are however those of the author(s) only and do not necessarily reflect those of the European Union or European Innovation Council and SMEs Executive Agency (EISMEA). Neither the European Union nor the granting authority can be held responsible for them.

Inspired by the edge of stability principle of computation, we searched for conditions allowing the eigenvalues of an input-free neural network to stay inside or at most at the boundary of the unit circle. The resulting necessary conditions are:

$$\text{if } \sigma > \xi - \gamma_{max}\text{, then } \sigma \leq \frac{1-\tau\,\gamma_{max}}{\tau+\tau^2}\text{;}$$

$$\text{if } \sigma \leq \xi - \gamma_{max}\text{, then } \sigma \leq \frac{1-\tau\,\xi}{\tau^2}\text{.}$$

We also derived necessary conditions on the stiffness and damping coefficients; namely, all of them being non-negative, while the maximum stiffness being less than the reciprocal of the discretisation time step, and the maximum damping coefficient being less than the squared reciprocal of the discretisation time step. We used all these weaker conditions as guideline values for training the neural network. Strikingly, the neural network was able to outperform standard RC models in classification tasks requiring long short-term memory while performing as good in forecasting of chaotic dynamical systems.

3.3 A network of PDM oscillators with potential coupling

Summary: PDM oscillators network contains the multiple PDM oscillators as units which are coupled by potential coupling connectors. The dynamics of the PDM oscillators are represented by the decoupled Euler-Lagrangian equation. We are interested in understanding if a small set of PDM oscillators is expressive enough to approximate the dynamic behaviour of a multi-body mechanical system (e.g., an n-pendulum). We approach the challenge by starting from the generic coupled system and propose a way of decoupling the mass resulting into an archetype network, defined as a collection of distinct and independent PDM oscillator units.

Definition: The dynamics of an unforced, n-link pendulum are given by

$$M(\xi)\ddot{\xi} + C(\xi,\dot{\xi})\dot{\xi} + G(\xi) = 0$$

where O is the number of links and $\xi \in R^O$ is the position (e.g., angles) of the links. Furthermore, $M \in R^{O\times O}$ is the inertia matrix, $C \in R^{O\times O}$ collects the Coriolis and centrifugal effects, and $G \in R^O$ is the gravity vector. We propose an encoder $\epsilon: \xi \to x$ that can find a mapping between the pendulum state ξ and the PDM oscillator configuration $x \in R^N$ and is also differentiable. The encoder facilitates the discovery of latent space dynamics that can be expressed by independent PDM oscillators. This, in turn, enables a refined analysis within a reduced-order space when $O > N$ or via the utilization of simplified dynamics equations. The encoder function allows us to find a relation between $\dot{\xi}$ and $\dot{x}$ as

$$\dot{x} = \frac{\partial \epsilon}{\partial \xi}\dot{\xi} = J_\epsilon(\xi)\dot{\xi}$$

where $x \in R^N, \dot{x} \in R^N$ is the position and velocity of all the PMD oscillators. Subsequently, to effect the inverse transformation from the latent space back to the original space, we deploy a decoder as D. This decoder maps from $x \to \xi$, thereby enabling us to obtain derivatives of the original state by

Funded by the European Union

European Innovation Council

Funded by the European Union under Grant Agreement 101070918. Views and opinions expressed are however those of the author(s) only and do not necessarily reflect those of the European Union or European Innovation Council and SMEs Executive Agency (EISMEA). Neither the European Union nor the granting authority can be held responsible for them.

$$\dot{\xi} = \frac{\partial D}{\partial x}\dot{x} = J_D(x)\dot{x}$$

This encoder-decoder framework allows a comprehensive exploration of the latent space dynamics while maintaining a connection to the original space. The encoder-decoder framework can take various forms, including Principal Component Analysis (PCA), Linear Regression, interpolation methods, or neural networks. In our specific examples, we employ neural networks as both the encoder and decoder. The loss function to train the encoder and decoder networks contains the following four parts:

$$\begin{aligned}
&\left\| J_\xi(\xi)M(\xi)J_\xi(\xi)^T - trace\left(J_\xi(\xi)M(\xi)J_\xi(\xi)^T\right)\right\|_2^2 \\
&+\left\| J_\xi(\xi)J_\xi(\xi)^T - I_{n\times n}\right\|_2^2 \\
&+\left\|\xi - D(\epsilon(\xi))\right\|_2^2 \\
&+\left\| J_\xi^T(\xi) - J_D(x)\right\|_2^2
\end{aligned}$$

The first part of the loss ensures the diagonal structure of the new mass matrix in the latent space. Since $M(\xi)$ is positive-definite, the second part, the relationship $J_\epsilon(\xi)^{-1} = J_\epsilon(\xi)^T$, will always remain valid. The final two components of the loss function are designed to capture the reconstruction error. After the coordinate transformation, the diagonal elements of the new mass matrix are still dependent on all configuration variables, so the Coriolis matrix still couples across these oscillator variables. The system's equilibrium point is utilized to approximate a decoupled Coriolis matrix.

$$m_i(\bar{x}, x_{k,i})\ddot{x}_{ki} + c_i(\bar{x}, x_{k,i}, \dot{x}_{k,i})\dot{x}_{ki} + g_i(x_k) = 0$$

where $\bar{x}$ is defined as $\bar{x} = \epsilon(\bar{\xi})$ and $\bar{\xi}$ is the system's equilibrium point.

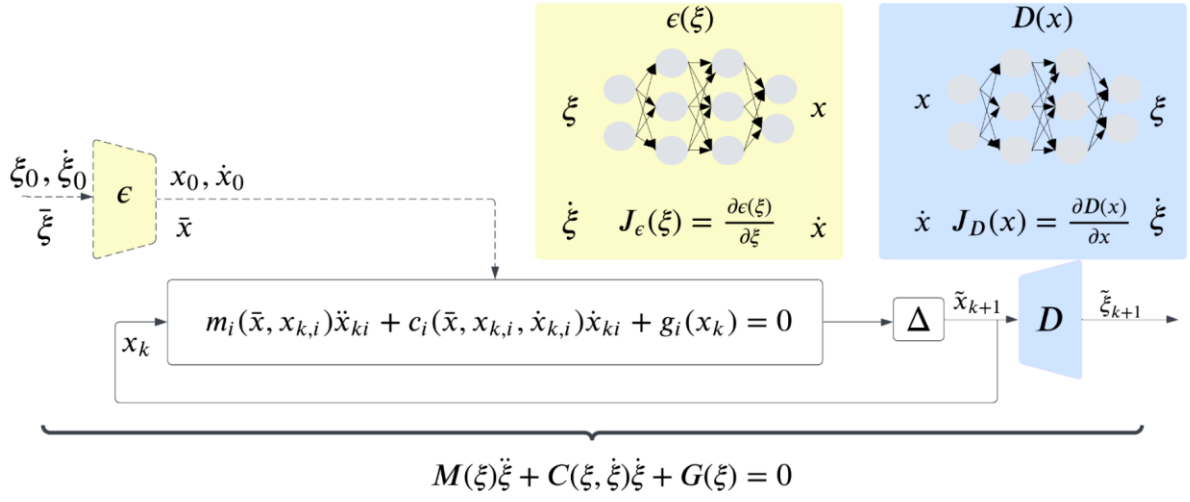

Figure 12: Block diagram for the computation of the PDM oscillator dynamics: the pendulum state, denoted as $(\xi, \dot{\xi})$, is mapped by an encoder (ϵ) into a PDM oscillator state, represented as $(x, \dot{x})$. The state at the next time step

Funded by the European Union

European Innovation Council

Funded by the European Union under Grant Agreement 101070918. Views and opinions expressed are however those of the author(s) only and do not necessarily reflect those of the European Union or European Innovation Council and SMEs Executive Agency (EISMEA). Neither the European Union nor the granting authority can be held responsible for them.

is computed by integrating $\ddot{x}$ with a fourth-order Runga-Kutta. The pendulum's future state is then recovered by a decoder (D).

Characterization:

To evaluate the effectiveness of this framework, we use it for analysing the latent space dynamics of a few nonlinear systems such as the double pendulum, and a triple pendulum.

The double pendulum system is a classic example of a simple mechanical system that exhibits complex and chaotic behaviour. It consists of two connected links, where each pendulum can swing freely in response to gravity and the motion of the other pendulum. The dynamics of the double pendulum are characterized by a coupling between its states, ξ_1 and ξ_2. Some sample time evolutions are shown in Figure 13.

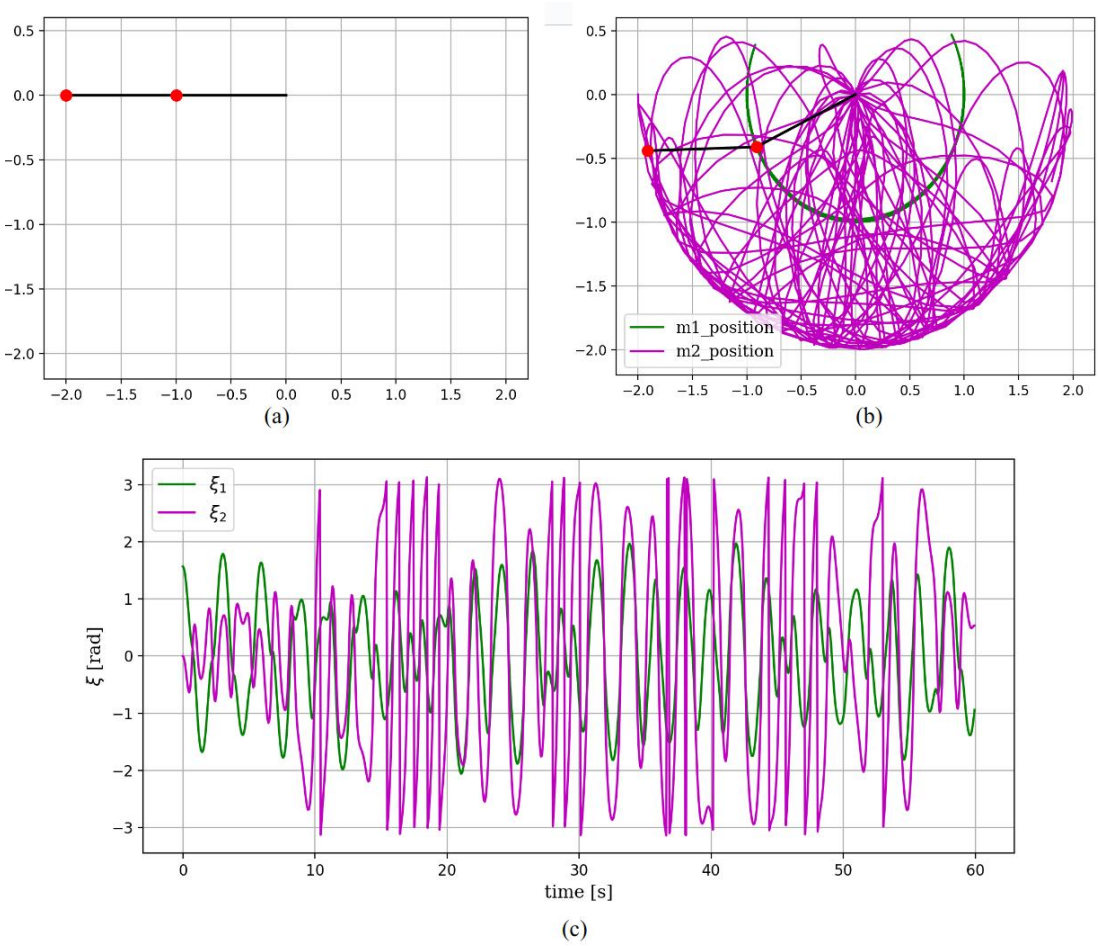

Figure 13: double pendulum simulation of 60 seconds duration with initial condition as$(\xi_1(0), \xi_2(0), \dot{\xi}_1(0), \dot{\xi}_2(0)) = (\frac{\pi}{2}, 0, 0, 0)$: (a) is the initial state of the simulation; (b) is the double pendulum trajectory; (c) is the time series plot of the state

The approximation of its motion can be achieved by employing PDM oscillators. The predictions of the PDM oscillators relative to the equilibrium point together with the actual system behaviour are shown in Figure 14.

Funded by the European Union

European Innovation Council

Funded by the European Union under Grant Agreement 101070918. Views and opinions expressed are however those of the author(s) only and do not necessarily reflect those of the European Union or European Innovation Council and SMEs Executive Agency (EISMEA). Neither the European Union nor the granting authority can be held responsible for them.

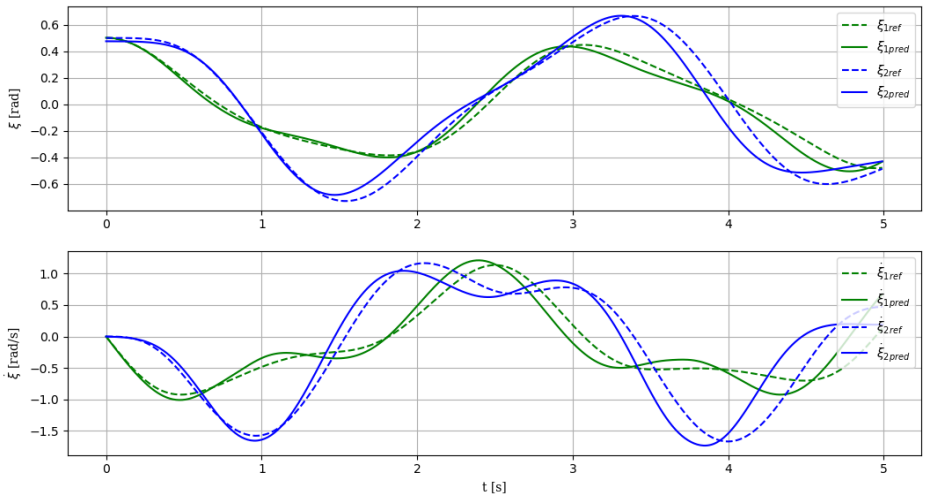

Figure 14: Double pendulum prediction results of the PDM oscillator network over 5-second interval simulation from the initial conditions (0.5, 0.5, 0.0, 0.0)

Given that the equilibrium point is employed for approximation, states closer to the equilibrium point yield more precise results. A similar predictive performance is evident in the case of the triple pendulum example in Figure 15, with a slight decrease in accuracy due to the considerably more intricate dynamics involved.

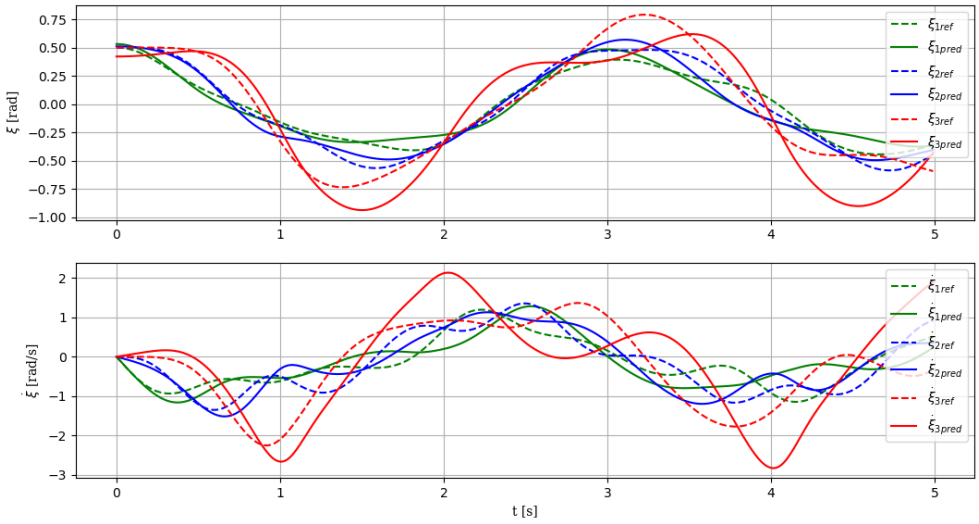

Figure 15: Triple pendulum prediction results of the PDM oscillator network over 5-second interval simulation from the initial conditions (0.5, 0.5, 0.5, 0.0, 0.0, 0.0)

Funded by the European Union

European Innovation Council

Funded by the European Union under Grant Agreement 101070918. Views and opinions expressed are however those of the author(s) only and do not necessarily reflect those of the European Union or European Innovation Council and SMEs Executive Agency (EISMEA). Neither the European Union nor the granting authority can be held responsible for them.

4 Towards an archetype-based computing and adapting system

The units and connectors defined so far, as well as the resulting networks, provide a substrate that can be used for computation and learning purposes. Networks of oscillatory units are particularly expressive (Rusch and Mishra 2021), hence particularly interesting for computational purposes. The full Archetype Computing System (ACS) and Archetype Adapting System (ADS) will be developed in WP4. Here, we briefly discuss the key points where the units/connectors and the ACS/ADS meet.

Computing with archetypes (ACS). The purpose of the ACS is to define how the units and connectors can be used to perform useful computation. The archetype units all define dynamical systems that evolve over time. The trajectory of a unit is therefore a direct response to the unit's state. The connectors include an externally provided input signal (the *global network inputs* v_s*)* that contributes to alter a unit's state.
In the ACS, computation can be performed by taking a set of units and connectors (i.e., a *network*) and by driving the network with the external input signal. The evolution of the state of the network, that is the joint evolution of all units, represents computation. Notwithstanding the network implementation, either in a digital or in an analogic/physical device, one can always monitor the evolution of the network's state in response to the input signal. The result of a computation performed over a time interval (discrete or continuous) is the output signal represented by the network's trajectory. This signal can be used to infer different properties of the input, for example by clustering the output trajectories in a low-dimensional space that contains semantic information about the different inputs. While the input space is often noisy, the state space of the trajectories usually allows to grasp qualitative and quantitative properties associated to the input.
Moreover, as discussed before, the formal definition of units and connectors allows to derive precise bounds on the behaviour of a given network, for example in terms of its stability or in terms of its state convergence properties (presence of attractors, types of attractors). While it is not possible to know in advance where a given input will drive the network trajectory, it is possible – and useful – to outline the set of possibilities for the network's evolution.
Computation is a first, fundamental step to *study* and *use* the archetypes defined in this document. One example of such kind of computation is represented by the Random Oscillators Network (RON) model (Ceni, et al. 2023) where a network of harmonic oscillators archetypes combined with hyperbolic potential connectors is shown to be able to solve a wide variety of different time-series tasks (e.g., classification, forecasting).

Learning with archetypes (ADS). The archetype units and connectors all depend on a set of parameters that control their behaviour. For example, a harmonic oscillator has parameters controlling the amount of damping and frequency of oscillation, while a neuron-like connector has parameters controlling the relative importance (*weight)* of the external input and of the internal network's state. These parameters highly influence the computation performed by a network. Consequently, being able to tweak these parameters towards interesting and useful configuration would allow to "*train"* the network to solve a particular problem. This is the objective of learning: finding a configuration of parameters that exploits the computation performed by a network for a certain objective. Learning in the ADS can be done in different ways: from gradient-based optimization of the parameters (LeCun, Bengio and Hinton 2015) to evolutionary algorithms that iteratively compare and select the best versions of a network among a set of candidate ones (Stanley, et al. 2019). Interestingly, the

Funded by the European Union

European Innovation Council

Funded by the European Union under Grant Agreement 101070918. Views and opinions expressed are however those of the author(s) only and do not necessarily reflect those of the European Union or European Innovation Council and SMEs Executive Agency (EISMEA). Neither the European Union nor the granting authority can be held responsible for them.

networks presented so far are all compatible with both forms of learning procedures. Existing techniques to learn with artificial neural networks can be directly used in this context (e.g., to train a network of harmonic oscillators with neural coupling) (Rusch and Mishra 2021) (Keller and Welling 2023), while new ones can be designed according to specific needs.

Funded by the European Union

European Innovation Council

Funded by the European Union under Grant Agreement 101070918. Views and opinions expressed are however those of the author(s) only and do not necessarily reflect those of the European Union or European Innovation Council and SMEs Executive Agency (EISMEA). Neither the European Union nor the granting authority can be held responsible for them.

Appearing in

In the following, we will list the content in this deliverable that has been already or is in preparation to be published in scientific proceedings or journals:

- **Section 3.1:** A work involving a physically implementable network of harmonic oscillators with hyperbolic coupling is currently under preparation for a journal submission (Ceni et al., under preparation)
- **Section 3.2:** The network of harmonic oscillators with neural coupling was presented at the ICML 2023 workshop on New Frontiers in Learning, Control, and Dynamical Systems (Ceni et al., 2023, Frontiers4LCD). This piece of research with an expanded experimental verification was also submitted to the 38th Annual AAAI Conference on Artificial Intelligence 2024 and is currently under review (Ceni et al., AAAI 2024).

Ceni, Andrea, Andrea Cossu, Jingyue Liu, Maximilian Stölzle, Cosimo Della Santina, Claudio Gallicchio, and Davide Bacciu. 2023. Randomly Coupled Oscillators for Time Series Processing. N.p.: ICML 2023 Workshop Frontiers4LCD. https://openreview.net/forum?id=fmn7PMykEb.

Andrea Ceni, Andrea Cossu, Maximilian Stölzle, Jingyue Liu, Cosimo Della Santina, Davide Bacciu, and Claudio Gallicchio, Random Oscillators Network for Time Series Processing, AAAI 2024, under review

Andrea Ceni, Andrea Cossu, Maximilian Stölzle, Jingyue Liu, Cosimo Della Santina, Davide Bacciu, and Claudio Gallicchio, Randomly Coupled Oscillators Networks for Time Series Processing, under preparation.

Funded by the European Union

European Innovation Council

Funded by the European Union under Grant Agreement 101070918. Views and opinions expressed are however those of the author(s) only and do not necessarily reflect those of the European Union or European Innovation Council and SMEs Executive Agency (EISMEA). Neither the European Union nor the granting authority can be held responsible for them.

Bibliography

Khalil, Hassan K. 2002. *Nonlinear systems.* Prentice Hall.

Wu, Xuwei, Christian Ott, Alin Albu-Schäffer, and Alexander Dietrich. 2022. "Passive Decoupled Multitask Controller for Redundant Robots." *IEEE Transactions on Control Systems Technology* 31 (1): 1-16.

Ceni, Andrea, Andrea Cossu, Jingyue Liu, Maximilian Stölzle, Cosimo Della Santina, Claudio Gallicchio, and Davide Bacciu. 2023. "Randomly Coupled Oscillators for Time Series Processing." ICML 2023 Workshop Frontiers4LCD, 05 26. https://openreview.net/forum?id=fmn7PMykEb.

P. M., Mathews, and Lakshmanan M. 1974. "On a unique nonlinear oscillator." *Quarterly of Applied Mathematics* 32 (32): 215-218.

Rusch, T. Konstantin, and Siddhartha Mishra. 2021. “Coupled Oscillatory Recurrent Neural Network (coRNN): An accurate and (gradient) stable architecture for learning long time dependencies.” *International Conference on Learning Representations (ICLR).*

Keller, T. Anderson, and Max Welling. 2023. “Neural Wave Machines: Learning Spatiotemporally Structured Representations with Locally Coupled Oscillatory Recurrent Neural Networks.” *40th International Conference on Machine Learning (PMLR 2023).* 16168-16189.

LeCun, Yann, Yoshua Bengio, and Geoffrey Hinton. 2015. "Deep Learning." *Nature* 436-444.

Stanley, Kenneth O., Jeff Clune, Joel Lehman, and Risto Miikkulainen. 2019. “Designing neural networks through neuroevolution.” *Nature Machine Intelligence* 24-35.

Funded by the European Union

European Innovation Council

Funded by the European Union under Grant Agreement 101070918. Views and opinions expressed are however those of the author(s) only and do not necessarily reflect those of the European Union or European Innovation Council and SMEs Executive Agency (EISMEA). Neither the European Union nor the granting authority can be held responsible for them.